Fast Ion Dynamics in TEXTOR measured by Collective Thomson Scattering

H Bindslev[ae], L Porte[b], J A Hoekzema[d], D van Eester[c],
A Messiaen[c], G Van Wassenhove[c] , P Woskov[b]
[a]FOM Instituut voor Plasmafysica, Rijnhuizen, The Netherlands*
[b]MIT Plasma Science and Fusion Center, Cambridge, MA, USA
[c]ERM/KMS, Brussels, Belgium*
[d]KFZ, Jülich, Germany*
[e]Now at EURATOM-Association Risø, Denmark
*EURATOM-Association and partner in the Trilateral Euregio Cluster (TEC)

The TEXTOR fast ion collective Thomson scattering (CTS) diagnostic[1] became operational August 2000. In 7 dedicated shot days just over 200 useful shots have been recorded in pursuit of both generic fast ion physics such as fast ion sawtooth sensitivity and confinement time, and specific Ion Cyclotron Resonance Heating (ICRH) physics issues intended to challenge and benchmark model calculations. The diagnostic is based on the scattering of probe radiation (110 GHz, 100 kW, 200 ms gyrotron) off the microscopic fluctuations driven by ions. The probe is launched near the outer midplane of the tokamak plasma, and scattered radiation detected in the same poloidal cross section, yielding a flexible near back scattering geometry. The CTS signal is distinguished from the background radiation by modulating the probe radiation as illustrated in Figure 1. The signal to noise ratio and system constraints currently permit the recording of CTS spectra in each shot at up to 100 time slices, 4 ms apart, each spectrum representing a 2 ms temporal average.

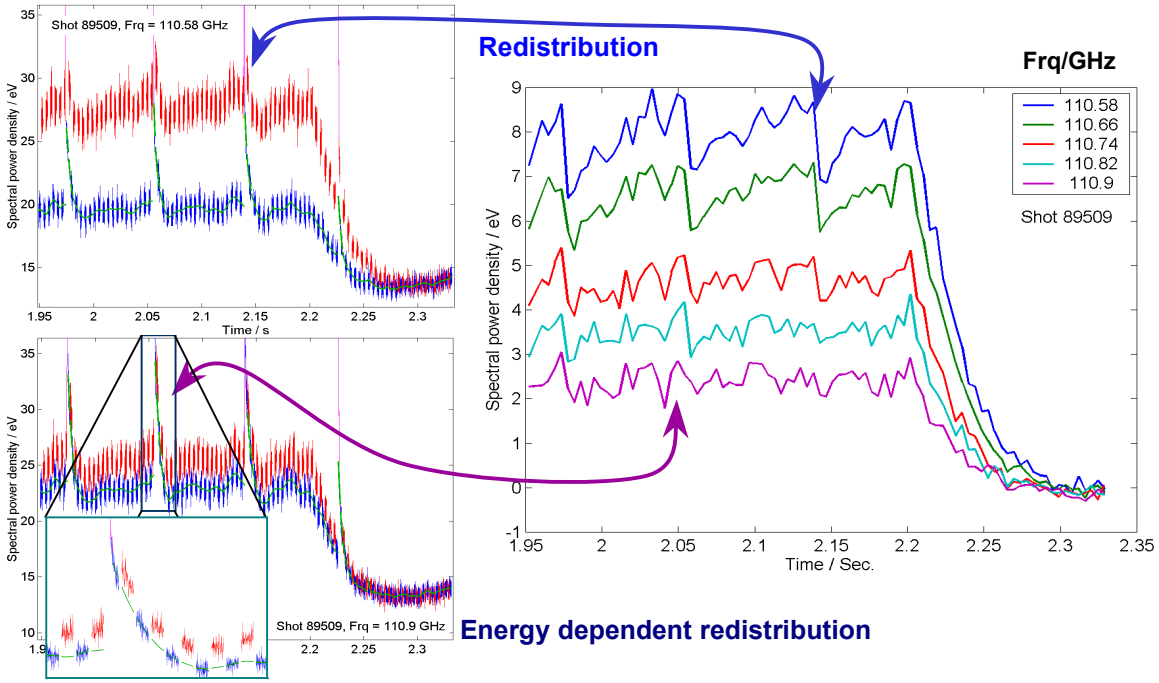

Figure 1 Shot 89509. Spectral power density (in eV) versus time (in seconds) recorded in a range of discrete spectral channels centred at 110.58 to 110.90 GHz. The left plots show the sampled calibrated data in two channels (109.58 and 110.90 GHz). Red (blue) samples are recorded when the probe radiation from the gyrotron is on (off). The background radiation level is estimated from the data recorded when probe is off (see fit in *close up*) and subtracted from the radiation recorded when the probe is on to estimate the spectral power density of the scattered radiation. The latter is plotted in the right plot.

The spectra are detected in 40 discrete frequency channels, 23 of which could be selected for recording. A typical set of spectral data is shown in Figure 2, where the effects of sawteeth and fast ion population decay at the end of the auxiliary heating period are apparent.

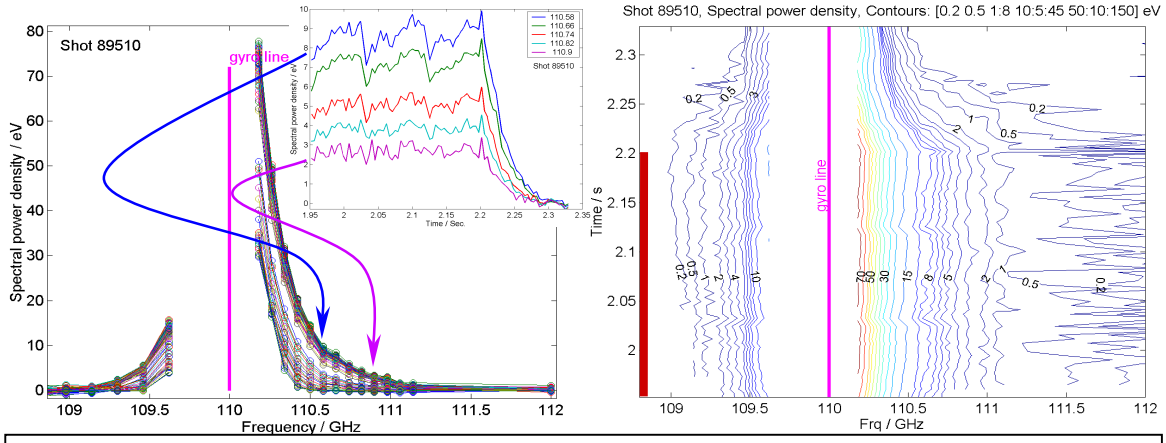

Figure 2 Spectral power density of received scattered radiation as functions of frequency and time. 90 spectra are recorded 4 ms apart, each spectrum representing a 2 ms temporal integration with probe on. Left the spectra are overlaid. Left inset shows time traces from selected channels. Right a contour plot of the spectral power density. Auxiliary heating (NBI and ICRH) was on till 2.2 seconds.

The CTS measurements are spatially localised by the overlap of probe and receiver beam patterns. With the current system the radial resolution is typically 10 cm, resolutions in other directions being better. The location of the measuring volume can by shifted by changing the pointing directions of probe and receiver beam patterns (scattering geometry). A given scattering geometry resolves the microscopic fluctuations with the wave vector, $\mathbf{k}^{\delta}$, which satisfies the Bragg condition. From the resulting CTS spectra the spatially localised, 1-D distribution of ion velocities along $\mathbf{k}^{\delta}$ can be inferred. Change of scattering geometry redirects $\mathbf{k}^{\delta}$ and hence the resolved ion velocity component, u. Varying the scattering geometry thus permits the study of anisotropy and spatial inhomogeneity of the ion distributions and their dynamics. As an example this capability is exploited to try to link ion sawtooth sensitivity to ion drift orbit class. We will discuss the results from the small selection of shots given in the table in Figure 3, where radial resolution and resolved velocity component are illustrated.

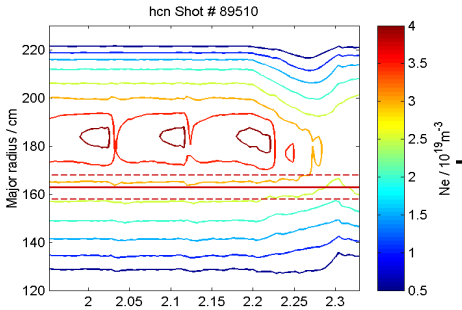

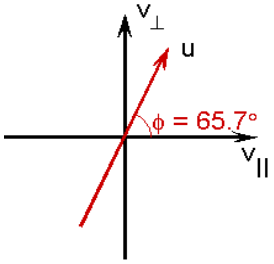

Shot #	R/cm	ϕ
89509	163	65.7°
89510	163	65.7°
89511	199	71.3°
89519	171	12.1°
89528	157	169.0°

Figure 3 Left, contour plot of electron density in plasma midplane as functions of major radius, R, and time. Solid straight line indicates centre of CTS measuring volume and parallel dashed lines its radial extent. Here (shot 89510) the volume is inside but near the electron density inversion radius. Central, a vector diagram indicating direction of the velocity component, u, resolved with a given scattering geometry. $v_{||}$ is parallel to the magnetic field, positive in the direction of the plasma current. $\phi = \angle(u, v_{||})$. Right, table giving major radius of scattering volume centre and direction of resolve velocity component for a range of selected shots.

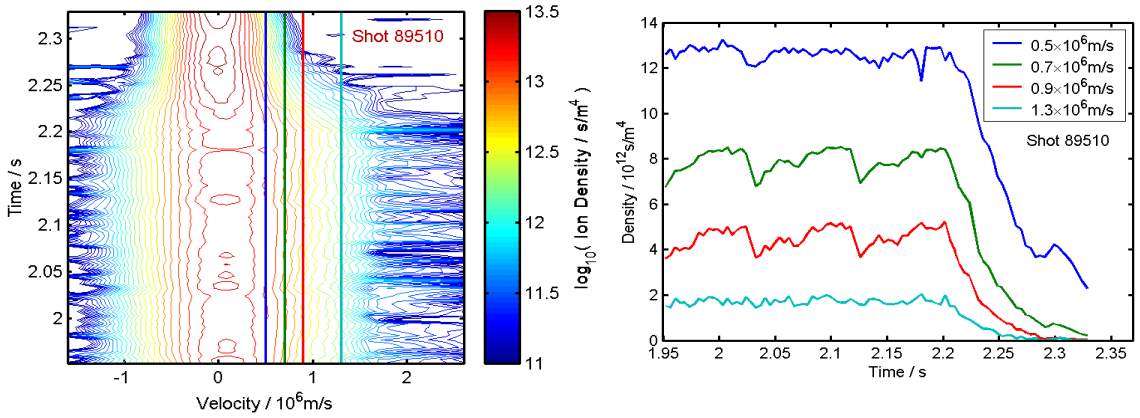

Figure 4 Shot 89510. Ion phase space density (particles per unit volume and unit velocity along resolved velocity component) as functions of velocity and time. Left log contour plot of phase space density, right time traces of density at selected velocities.

An example of a 1-D velocity distribution inferred from CTS is shown in Figure 4. In this shot the measuring volume was on the high field side of the plasma centre and just inside the electron density sawtooth inversion radius (Figure 3, left). The resolved ion velocity component is near perpendicular to the magnetic field (Figure 3, centre). The auxiliary heating (NBI and ICRH) was switched off at 2.2 seconds, after which the fast ion population is seen to decay to nothing in approximately than 100 ms. This is in good agreement with the estimated ion slowing down time due to electron drag (45 ms).

With the achieved temporal resolution, ion dynamics associated with sawteeth is also resolved. To estimate the changes in the ion population at sawteeth we fit the ion phase space density time series as illustrated in Figure 5 and record the steps in the fits. The ion population sawtooth step as a function of ion velocity is also shown in Figure 5, as is the step normalized by the population density. The latter gives the fractional change in population density at a given velocity. Negative values correspond to loss of ions. There is a notable maximum loss of 30 % near ion velocities of 10^6m/s. At higher velocities the fractional loss reduces to near zero, and at lower velocities the changes become positive.

Changing the scattering geometry, the distribution as a function of velocity components near parallel to the magnetic field are resolved at approximately the same major radius (shots 89519 and 89528). The relative sawtooth step curves for these two shots are overlaied that from shot 89510 in the lower right plot in Figure 5. There is a very notable reduction in the sawtooth losses fraction when near parallel velocities are resolved. Note that in shot 89519 the geometry is such that the beam ion tail appears at positive velocities while in 89528 it appears at negative velocities. The curves for the two shots extend furthest in the side where the beam tail is, since at low population densities the uncertainty in the fractional change becomes large and is not plotted. The data from these three shots is consisten with a loss of fast ions from velocity space islands living within a narrow range of pitch angles near perpendicular, as illustrated in Figure 6.

Further information on which ion drift orbits are susceptible to sawtooth activity is gained from measurements at other poloidal locations. In shot 89511 the measurement volume was at the mid plane, on the low field side of the centre. Again near the n_e inversion radius. In this shot a near perpendicular velocity component is resolved as in shot 89510. But unlike that previous shot, in 89511 we find very little sawtooth activity in the ion velocity distribution as demonstrated by the normalised step curve for shot 89511 in Figure 5, bottom right. So, a notable difference between high and low field side of centre.

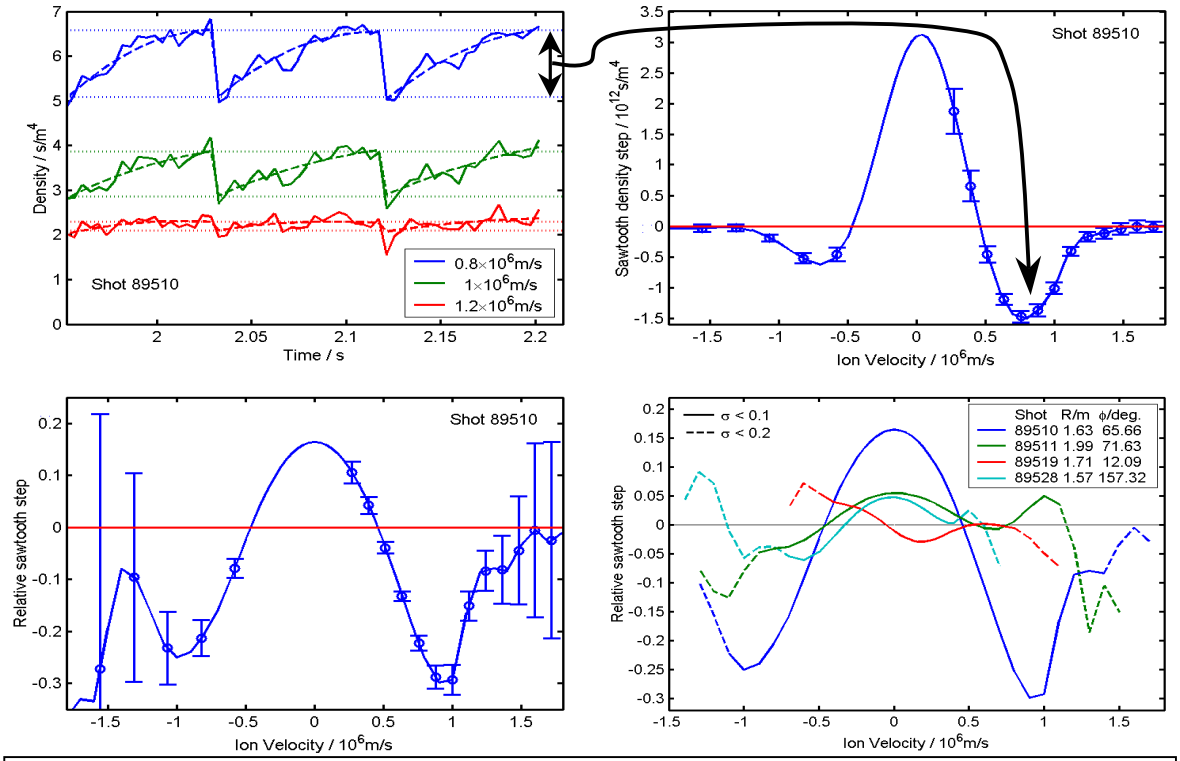

Figure 5 Sawteething of the ion phase space distribution. Shot 89510. Top left, polynomial fit to extract sawtooth step, negative for loss. Top right, sawtooth step as a function of velocity. Bottom left, sawtooth step normalised by phase space density to give relative sawtooth step. Bottom right, relative sawtooth step for four shots resolving different velocity components and at different radial locations, see Figure 3.

Figure 6 Suggested sawtooth loss region of velocity space, for spatial locations at the midplane, on the high field side near plasma centre. The indicated loss regions are consistent with the data from shots 89510, 89519 and 89528 which resolve respectively the velocity distributions near parallel and near perpendicular the magnetic field (see Figure 3).

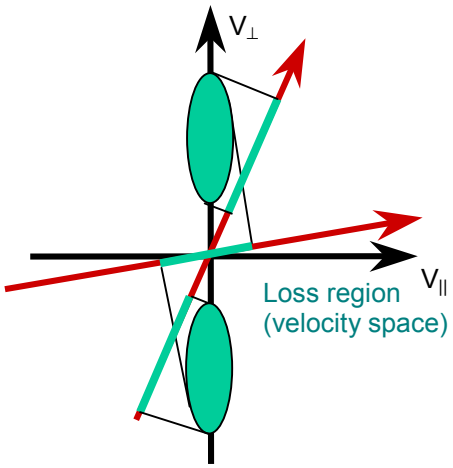

In conclusion, while only a small fraction of our new data could be discussed here, we hope the capabilities of fast ion CTS are demonstrating their appeal.

References

[1]TEXTOR fast ion CTS home page: http://www.rijnh.nl/users/bindslev/CTS. H. Bindslev, L. Porte, A. Hoekzema, J. Machuzak, P. Woskov, D. van Eester, 26th EPS Conf. Contr. Fusion and Plasma Physics, Maastricht, Netherlands, Vol. 23J, part II, p765, EPS (1999); H. Bindslev, L. Porte, A. Hoekzema, J. Machuzak, P. Woskov, D. van Eester, J. Egedal, J. Fessey, T. Hughes, *Fusion Engineering and Design*, **53**, 105 (2001); H. Bindslev, Journal of Plasma and Fusion Research. 76, 878 (2000); L. Porte, H. Bindslev, F. Hoekzema, J. Machuzak, P. Woskov, and D. Van Eester, Review of Scientific Instruments **72**, 1148 (2001); L Porte, H Bindslev et al., P1.110 *ibid*.